Mesoscale circulations and atmospheric CO_2 variations in the Tapajós Region, Pará, Brazil

Lixin Lu,[1] A. Scott Denning,[1] Maria Assuncao da Silva-Dias,[2,3] Pedro da Silva-Dias,[2] Marcos Longo,[2] Saulo R. Freitas,[3] and Sassan Saatchi[4]

Received 31 December 2004; revised 19 May 2005; accepted 4 August 2005; published 2 November 2005.

[1] We have investigated mesoscale circulations and atmospheric CO_2 variations over a heterogeneous landscape of forests, pastures, and large rivers during the Santarém Mesoscale Campaign (SMC) of August 2001. The atmospheric CO_2 concentration variations were simulated using the Colorado State University Regional Atmospheric Modeling System with four nested grids that included a 1-km finest grid centered on the Tapajós National Forest. Surface CO_2 fluxes were prescribed using idealized diurnal cycles over forest and pasture that derived from flux tower observations; while surface water CO_2 efflux was prescribed using a value suggested by in situ measurements in the Amazon region. Our simulation ran from 1 August through 15 August 2001, which was concurrent with the SMC. Evaluation against flux tower observations and Belterra meteorological tower measurements showed that the model captured the observed 2-m temperatures and 10-m winds reasonably well. At 57 m the model reproduced the daytime CO_2 concentration better than the nighttime concentration but missed the observed early morning CO_2 maxima, in part because of the difficulties of simulating stable nocturnal boundary conditions and subgrid-scale intracanopy processes. The results also suggested that the topography, the differences in roughness length between water and land, the "T" shape juxtaposition of Amazon and Tapajós Rivers, and the resulting horizontal and vertical wind shears all facilitated the generation of local mesoscale circulations. Possible mechanisms producing a low-level convergence (LLC) line near the east bank of the Tapajós River were explored. Under strong trade wind conditions, mechanical forcing is more important than thermal forcing in LLC formation. Persistent clouds near the east side of the Tapajós River may have a significant impact on observed ecosystem carbon flux and should be taken into account if tower fluxes are to be generalized to a larger region.

Citation: Lu, L., A. S. Denning, M. A. da Silva-Dias, P. da Silva-Dias, M. Longo, S. R. Freitas, and S. Saatchi (2005), Mesoscale circulations and atmospheric CO_2 variations in the Tapajós Region, Pará, Brazil, *J. Geophys. Res.*, *110*, D21102, doi:10.1029/2004JD005757.

1. Introduction

[2] The Amazon Basin plays a crucial role in global energy, water, carbon, and trace gas budgets [*Dickinson*, 1987]. Understanding and quantifying atmosphere-biosphere exchanges of heat, water, momentum, and CO_2 at scales from the plot up to the entire basin, is of major research interest to both carbon scientists and physical meteorologists. The Large Scale Biosphere-Atmosphere Experiment in Amazonia (LBA), launched as an international research initiative led by Brazil in 1997, aims to document the Amazon's present state as a regional entity using in situ data and analysis, and provide insight into its possible future changes through process-based numerical modeling. As part of the LBA program, the Santarém Mesoscale field Campaign (SMC) was carried out during the dry season of 2001 [*Silva Dias et al.*, 2004; D. R. Fitzjarrald et al., manuscript in preparation, 2005]. It provided a test bed for scientists coming from multidisciplinary backgrounds to exercise regional integration using information from flux tower and light aircraft measurements, meteorological observations, and mesoscale numerical modeling.

[3] Dry season meteorology in the Santarém region is characterized by persistent Trade Winds, but topographic and surface variations in the Tapajós region produce mesoscale circulations that have been documented from field data and satellite imagery [*Silva Dias et al.*, 2004; D. R.

[1]Department of Atmospheric Science, Colorado State University, Fort Collins, Colorado, USA.
[2]Department of Atmospheric Sciences, University of São Paulo, São Paulo, Brazil.
[3]Centre for Weather Forecasting and Climate Studies, National Institute for Space Research, Cachoeira Paulista, Brazil.
[4]NASA Jet Propulsion Laboratory, Pasadena, California, USA.

0148-0227/05/2004JD005757$09.00

Table 1. Model Options Used in the Study

Category	Options Selected	References
Basic equations	nonhydrostatic, compressible	*Tripoli and Cotton* [1980]
Vertical coordinates	terrain-following sigma z	*Clark* [1977] and *Tripoli and Cotton* [1982]
Horizontal coordinates	oblique polar-stereographic projection	
Grid stagger and structure	Arakawa C grid, multiple nested grid (fixed)	*Arakawa and Lamb* [1977]
Time differencing	hybrid	
Microphysics	bulk microphysics (single moment)	*Walko et al.* [1995]
Convective parameterization	modified-Kuo for grids 1 and 2	*Tremback* [1990]
Radiation	Harrington	*Harrington et al.* [1999, 2000]
Surface layer	Louis	*Louis* [1979] and *Louis et al.* [1982]
	LEAF-2, prognostic soil and vegetation model	*Walko et al.* [2000]
CO_2 fluxes	prescribed diurnal variation of GPP and respiration	flux tower data (Km 67 and Km 77)
	river CO_2 efflux	*Richey et al.* [1990]

Fitzjarrald et al., manuscript in preparation, 2005]. These include a shallow diurnal river breeze circulation forced by differential heating between the forest and the Tapajós and Amazon Rivers during trade wind breaks [*Silva Dias et al.*, 2004]. The trade wind break is frequently associated with a cold air mass intrusion into Amazonia, which is locally known as the "friagem" event [*Hamilton and Tarifa*, 1978; *Marengo et al.*, 1997]. The typical sequence of the event, as described by *Silva Dias et al.* [2004], begins with a midlatitude upper level trough, with an accompanying surface front and high-pressure area behind it, the latter with a northward continental trajectory. The south to southeasterly flow ahead of the high reaches of western Amazonia, significantly slows the surface and midlevel winds, and reduces average daily temperatures by several degrees Celsius (D. R. Fitzjarrald et al., manuscript in preparation, 2005).

[4] Local mesoscale circulation patterns, which are of great importance to regional climate [*Avissar and Pielke*, 1989; *Liu et al.*, 1999; *Hahmann and Dickinson*, 2001; *Lu and Shuttleworth*, 2002; *Xue et al.*, 2001], landscape hydrology [*Ludwig et al.*, 2003], flux tower measurement interpretation [*Baldocchi et al.*, 2001; *Baldocchi*, 2003], regional upscaling, and inverse modeling [*Stohl et al.*, 1995], are often closely linked to distinct landscape features and land cover heterogeneity. To help interpret observational data collected during the LBA SMC field campaign, we performed mesoscale numerical experiments using the Colorado State University (CSU) Regional Atmospheric Modeling System (RAMS). Several modifications were made to RAMS to include three-dimensional CO_2 transport, prescribed land-cover-specific, diurnal-varying surface CO_2 fluxes, and the effects of deep convective mass transport (CO_2RAMS). Our major goals were: (1) to evaluate whether CO_2RAMS is capable of reproducing the observed meteorology and atmospheric CO_2 concentration field; (2) to identify and analyze the mesoscale circulation patterns in the Santarém area; and (3) to examine their influences on the surface exchanges of energy, water, and CO_2 as observed at local flux towers.

[5] RAMS has been widely used in studies investigating the role of landscape variability and change in generating mesoscale circulations [*Pielke et al.*, 1991, 1993a, 1993b, 1998, 1999a, 1999b; *Stohlgren et al.*, 1998; *Lu et al.*, 2001; *Lu and Shuttleworth*, 2002]. It has been recognized as suitable for regional-scale weather and climate studies, and for its ability to capture mesoscale circulations resulting from a variety of heterogeneous land surface features [*Chen et al.*, 2001; *Pielke*, 2001].

[6] RAMS has also been applied to Southern Hemisphere studies. *Silva Dias et al.* [2004] performed a high-resolution (2-km grid increment) RAMS simulation over the Santarém area during weak trade wind episodes in July 2001. They found that the Tapajós River breeze induces a westerly flow contributing to the shallow cumulus formed on the east bank of the Tapajós River. *Freitas et al.* [2000, 2005], used RAMS, coupled with University of Sao Paulo's Trajectory Model, to forecast trace gas transport for Cooperative LBA Airborne Experiment (CLAIRE). They included the effects of subgrid-scale moist convective processes on tracer transport, so that the air parcel can be vertically transported to the cumulus top at the short timescale associated with

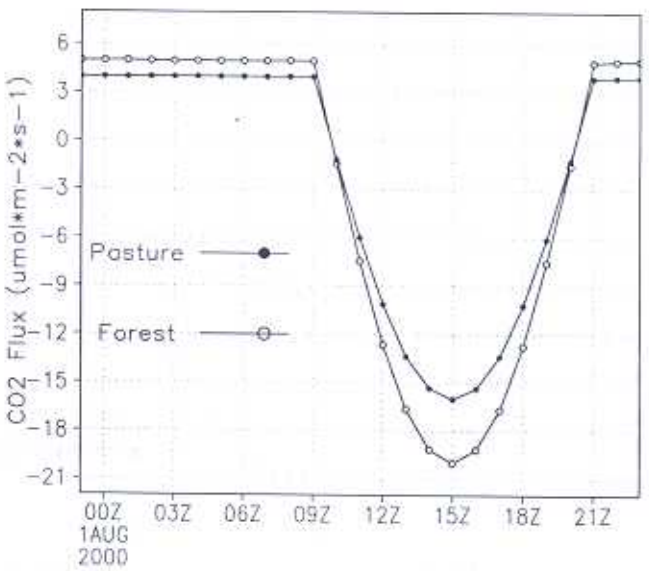

Figure 1. Prescribed diurnal variations of CO_2 fluxes for pasture and forest.

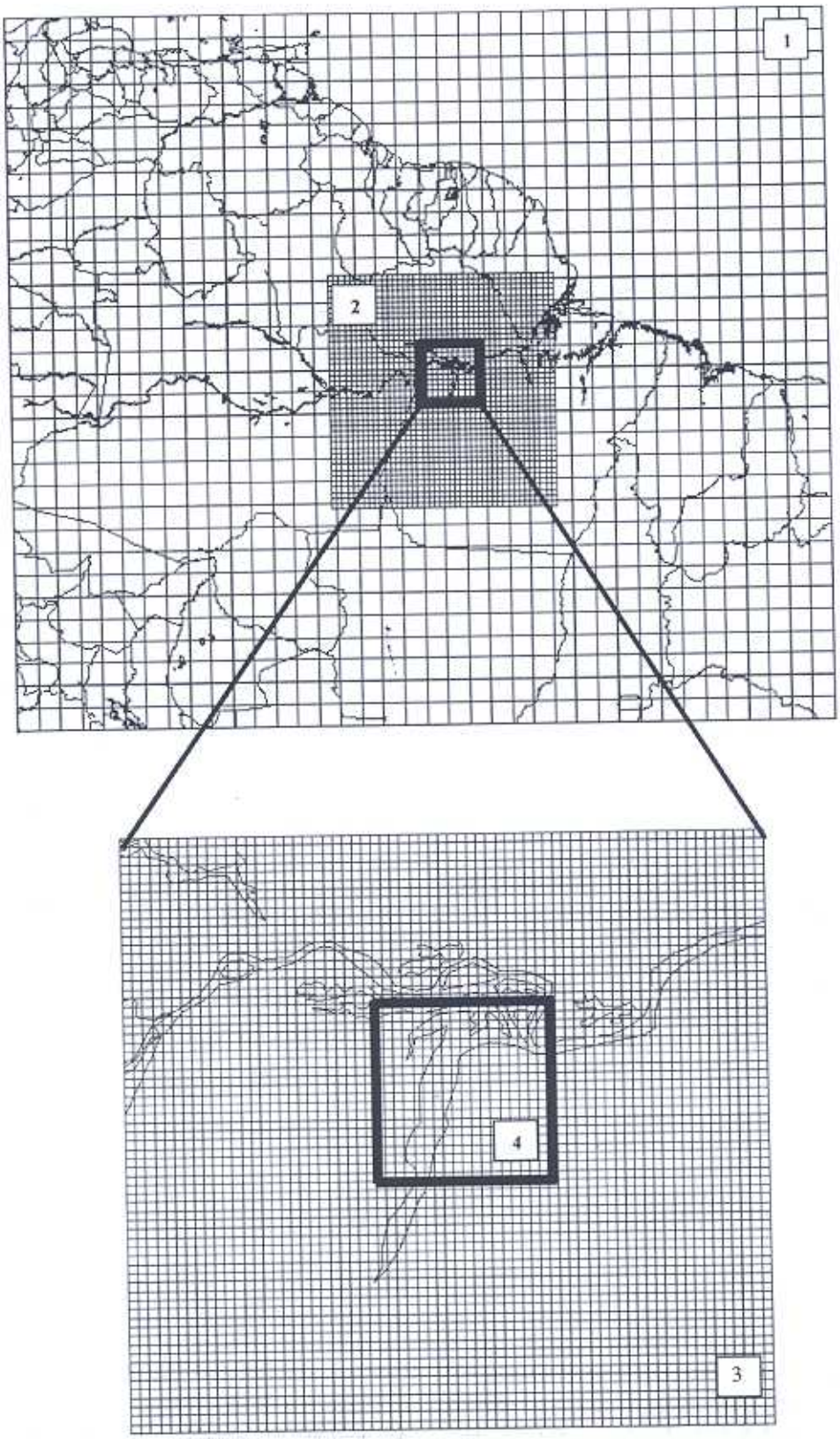

Figure 2. Model simulation domain and grid configuration of four nested grids. The coarsest to the finest grid intervals are 100 km, 25 km, 5 km, and 1 km, respectively. The 1-km grid increments of the inner grid are omitted for clarity. The pole point for the oblique polar stereographic projection for each grid is (−2.8°, −55.0°).

Table 2. Grid Parameters

Grid	$\Delta x = \Delta y$, km	Stretched Δz, m	Grid Dimensions	Δt, s
1	100	120~1000 (0~13 km) 1000 (13~25 km)	$38 \times 32 \times 32$ ($3800 \times 3200 \times 25$ km^3)	150
2	25	–	$42 \times 42 \times 32$ ($1050 \times 1050 \times 25$ km^3)	30
3	5	–	$67 \times 67 \times 32$ ($335 \times 335 \times 25$ km^3)	15
4	1	–	$97 \times 97 \times 32$ ($97 \times 97 \times 25$ km^3)	5

cumulus updrafts. Their results showed that their new transport scheme led to improved trajectory calculations when compared with satellite images and aircraft observations.

[7] More recently, RAMS has been employed in regional carbon budget studies. *Denning et al.* [2003] investigated the influence of ecosystem fluxes on atmospheric CO_2 in the vicinity of the WLEF-TV tower in Wisconsin using an ecophysiological model (SiB2) coupled to RAMS. They found the model was able to reproduce observed diurnal cycles of fluxes and concentration gradients, but revealed problems during transitions at sunrise and sunset that might be related to the canopy radiation parameterization in SiB2. In a similar study, *Nicholls et al.* [2004] further showed that katabatic winds, vertical wind shear, and circulations in the vicinity of lakes, caused variations in CO_2 concentration. These studies, along with our current study, span a range of different ecosystems and climatic zones around the world and provide examples of extrapolating local field observations of carbon fluxes and concentrations to large scales using numerical models and other spatial data products.

[8] Our paper is organized as follows: the atmospheric model, the physical parameterizations used, and the major changes made for the current study, are introduced in section 2. Also included in this section are the model grid configurations and numerical experiment design. In section 3, we describe the observational data and sites, and summarize the synoptic situation during the numerical experiment. In section 4, we first evaluate the modeled meteorological variables and atmospheric CO_2 concentration distribution against tower observations; second, we analyze the model results, focusing on the simulated vertical and horizontal spatial distribution of CO_2; and finally, the role of mechanical forcing versus thermal forcing in the formation of the low-level convergence (LLC) zone near the east bank of Tapajós River is explored. Discussion, conclusions, and future research directions are presented in section 5.

2. Model Description and Numerical Experiment Design

2.1. CO_2RAMS

[9] Regional Atmospheric Modeling System (RAMS) [*Pielke et al.*, 1992; *Cotton et al.*, 2003] Version 4.3 was adopted as our base model. The model's physical setup and parameterization options are summarized in Table 1.

[10] Several modifications were made to the base model to build CO_2RAMS. First, we introduced CO_2 exchanges between the atmosphere and land surface. To account for the complex spatial and temporal distributions of CO_2 surface fluxes, diurnally varying CO_2 fluxes were included as functions of local time and land cover type. Shown in Figure 1 are the diurnal cycles of surface CO_2 fluxes for pasture and forest. Maximum photosynthesis and respiration rate were prescribed separately according to vegetation type, which were derived from flux tower observations of the net ecosystem exchange (NEE) (eddy covariance flux towers Km 67, Km 77, and Km 83 located in Tapajós National Forest, Pará, Brazil). Respiration was defined to be constant in time because of the relatively small diurnal soil temperature variations in this moist study area; photosynthesis was assumed to vary sinusoidally on the basis of time of day. A constant flux of 5 μmol m^{-2} s^{-1} over inland water [*Richey et al.*, 1990, 2002] was specified for the surface water CO_2 effluxes. In this way, the spatial and temporal structures of surface carbon fluxes were constructed. Second, we implemented three-dimensional CO_2 transport associated with the surface CO_2 flux specifications. Finally, the *Freitas et al.* [2000] convective transport scheme was implemented to account for CO_2 transport via tropical deep convection. This scheme allows an air parcel associated with a convective updraft to reach the top of cumulus clouds on a much shorter timescale.

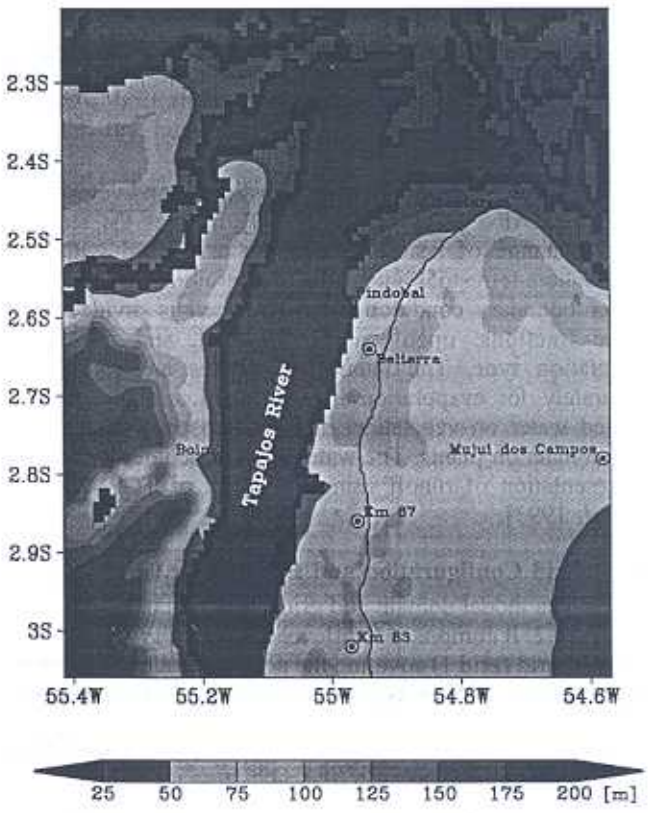

Figure 3a. Topographic distribution and location map of grid 4, the finest grid.

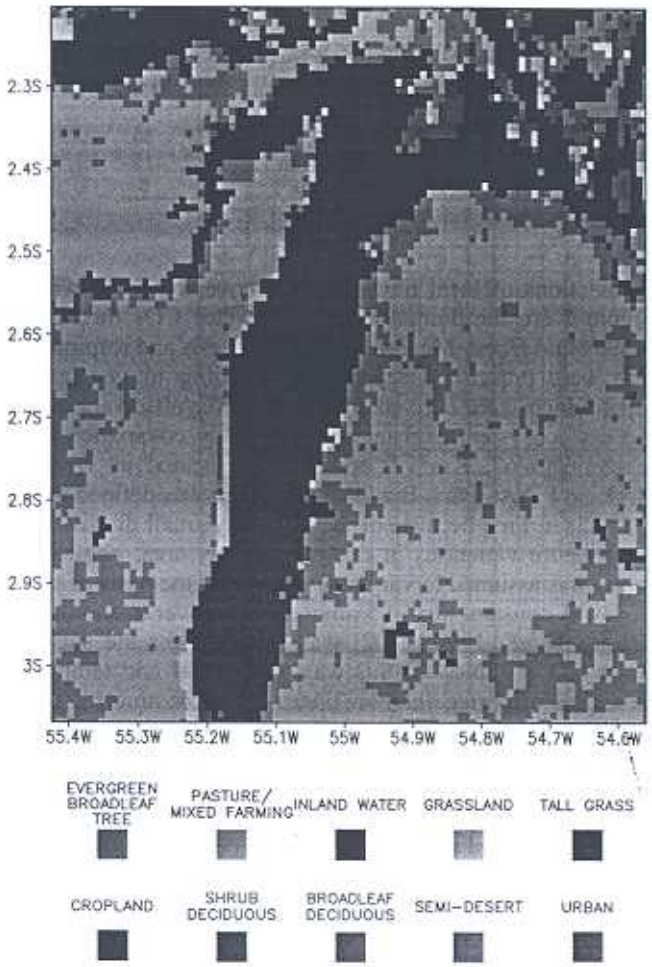

Figure 3b. Vegetation distribution of grid 4, the finest grid.

[11] At the land surface, a prognostic soil and vegetation model, LEAF-2 [*Walko et al.*, 2000], handles the storage and exchange of heat and moisture associated with the atmosphere-terrestrial interface, and provides the RAMS lower boundary condition. Each grid cell is divided into three fractions: open water, bare soil, and dominant vegetation type. The latent heat fluxes are calculated separately for evaporation from the soil and from intercepted water on vegetation, and for transpiration through the stomata on plants. The water budget includes a subgrid representation of runoff using a version of TOPMODEL [*Band*, 1993].

2.2. Grid Configuration and Experiment Design

[12] The model domain and grid configuration are shown in Figure 2. It comprises four levels of nested grids with the coarsest grid (grid 1) covering the northeastern part of South America and adjacent oceans at 100 km grid spacing, and the finest grid (grid 4) covering an area of 97 km × 97 km, focusing on the Santarém area at 1 km grid increment. The detailed information of each grid, including the vertical grid increment and time step, is listed in Table 2. The pole point for the oblique polar stereographic projection used to define grid 4 is 2.8°S and 55°W. The model is driven by 6-hourly lateral boundary conditions derived from Centro de Previsão de Tempo e Estudos Climáticos (CPTEC, i.e., Center for Weather Forecasts and Climate Research in Brazil) analysis products. Lateral boundary condition nudging is performed on the three outer boundary grid columns of the coarsest grid. The information provided at the lateral boundary includes horizontal wind speed, relative humidity, air temperature, and geopotential height on pressure levels.

[13] Driven by CPTEC analysis, CO_2RAMS was first used for a two-month (1 June through 31 July 2001) simulation with only two outer grids (grids 1 and 2) to allow the soil moistures and temperatures to adjust to model equilibrium. Then, using the end of July atmospheric and land surface states as an initial condition, we performed the four-nested-grid simulation with the finest grid at 1 km grid spacing. The experiment started on the 1 August 2001 and ended on 15 August 2001, concurrent with the Santarém mesoscale field campaign.

[14] Topographic features of our finest grid are rather distinct, as shown in Figure 3a. The Amazon and Tapajós Rivers form a "T" shape confluence in the center of our domain. In the east-west direction, the Tapajós River is approximately 15 km across. The southwest quadrant is higher than the rest of the domain, between 100 m and 200 m.

[15] Heterogeneous vegetation types, derived from the 1 km International Geosphere-Biosphere Programme (IGBP) land cover data set [*Loveland et al.*, 2000], were applied to the domain. Shown in Figure 3b is the vegetation map of our finest grid. The dominant land cover type is pasture and mixed farming, making up 51% of the domain. Inland water covers 27% of the area, evergreen broad leaf trees 17%; other land use types cover 5%. The IGBP 1 km land cover data set, both versions 1.2 and 2.0, have some unrealistic vegetation classes for the Amazon basin, which need corrections for high-resolution simulations in this area. *Saatchi et al.*'s [2000] data set, derived from Japanese Earth Resources Satellite–1 (JERS-1) L-band synthetic aperture radar mosaic products (100 m resolution), adequately represents the land surface heterogeneity of the Amazon Basin at 1 km, and provided us with additional land cover information.

[16] The initial and lateral boundary CO_2 concentrations were set to 360 ppm. In reality, the background CO_2 concentrations should change at the lateral boundaries from processes occurring outside the domain. However, in this experiment, we focus on short-term variability, i.e., the diurnal cycle of $[CO_2]$, not the synoptic variations. Quantitatively speaking, the diurnal $[CO_2]$ variation signals are about ten times larger than the lateral boundary $[CO_2]$ variations. In addition, only the fourth two-way nested grid is used for analysis. Therefore we consider it reasonable to use a fixed CO_2 lateral boundary concentration on the coarsest grid for the purposes of our study.

3. Observations, Site Description, and Synoptic Situation of August 2001

[17] As part of the LBA program, the Santarém Mesoscale Campaign was carried out during the early dry season

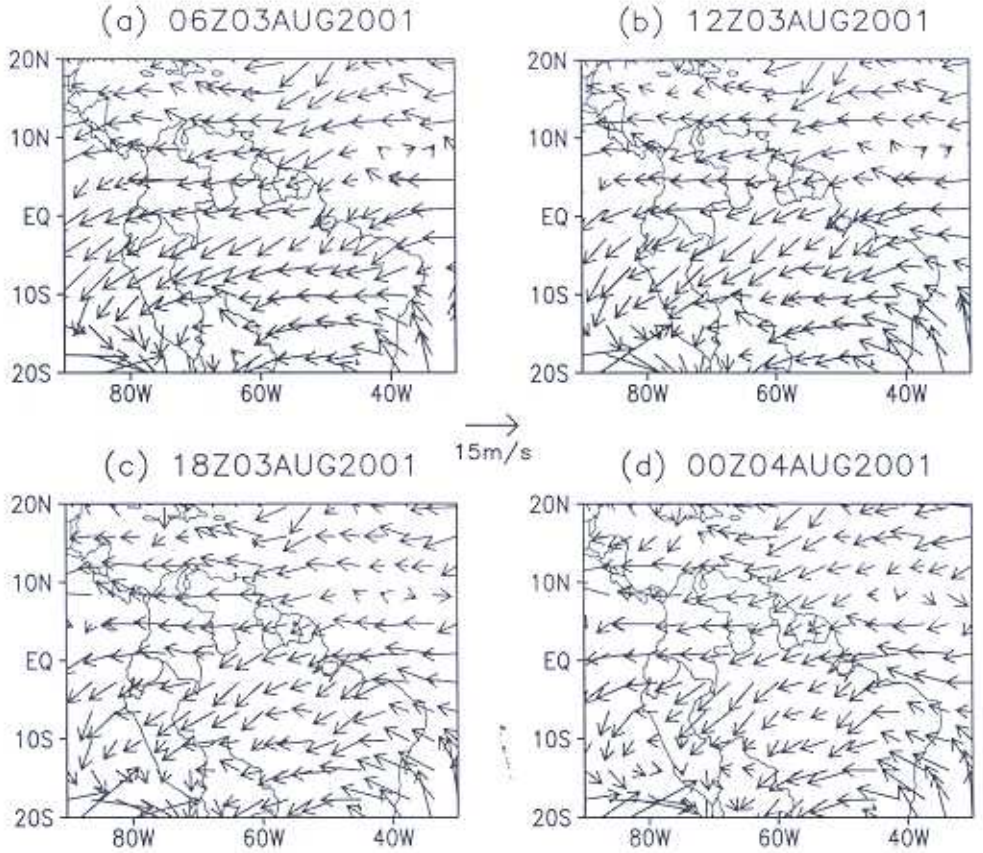

Figure 4. CPTEC 500 mbar analysis of horizontal wind vectors at 0600, 1200, 1800, and 2400 UT on 3 August 2001.

of 2001, to study the local circulation patterns in this area (Figure 3a). The red line across the north-south direction of the domain is Brazil Highway 163. On the east side of the Tapajós River and along both sides of Highway BR163, the eddy covariance flux towers (including Km 67, Km 77, and Km 83) operated by several LBA science groups, measured fluxes of heat, moisture, and trace gases as well as pressure, temperature, humidity, wind speed, and radiation profiles at

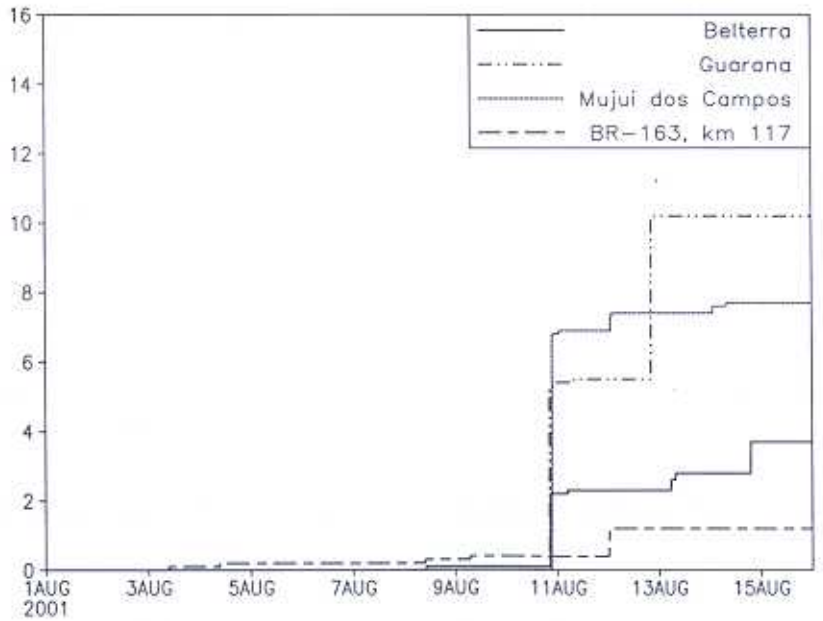

Figure 5. Observed accumulated precipitation on 1 through 15 August 2001 from automatic weather stations located in western Pará.

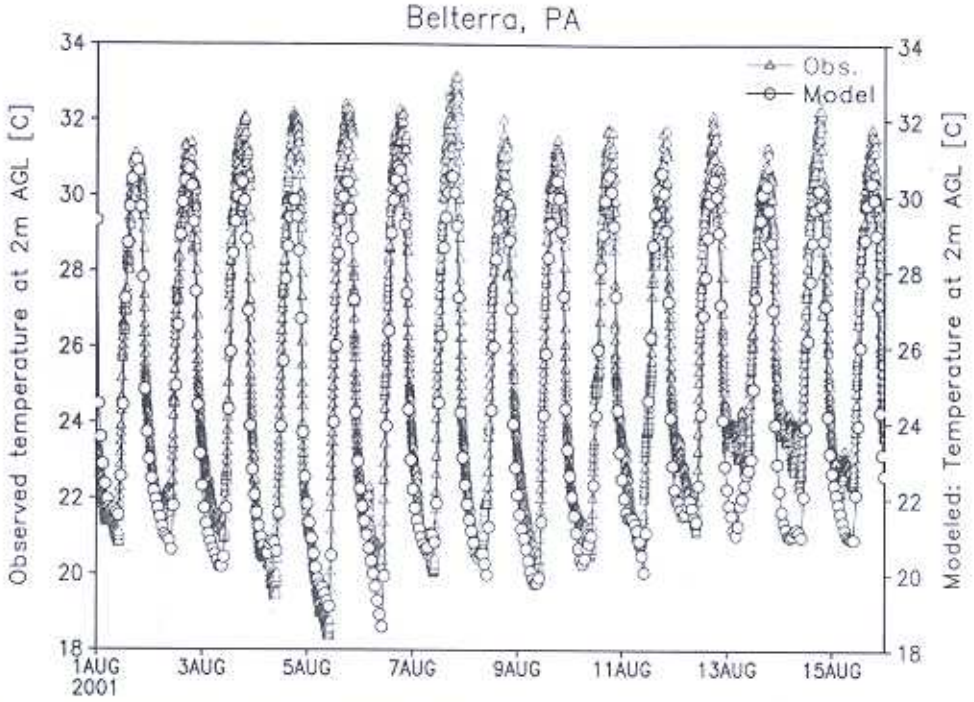

Figure 6. Modeled versus observed screen height 2-m air temperature. The times in the figure are in universal time (UT). The modeled output is at an hourly interval, while the observations are at a 5-min interval.

below and above the forest canopy levels [*Saleska et al.*, 2003]. A network of automatic weather stations, micrometeorological towers, light aircraft, sonic radars, radiosonde, and pilot balloons were deployed during the same time period. Detailed descriptions of the field campaign and other observational resources are given by *Silva Dias et al.* [2004].

[18] The observational sites used for model evaluation are as follows: the 10-m Meteorological Tower Station at Belterra, Pará, is located at latitude 2.646°S, and longitude 54.944°W, approximately 30 km southwest of Santarém (Figure 3a); the eddy covariance flux tower Km 67 (primary forest site) is located at latitude 2.855°S and longitude 55.036°W, southwest of Belterra station. Both observation sites are located near the east bank of Tapajós River, and Highway BR163 borders them to the east. Continuous records of the entire simulation time period are available from both sites.

[19] The synoptic situation for our simulation time period, 1 August through 15 August 2001, can be summarized as follows: intense trade winds blew almost constantly, with slight variations in wind directions, as shown in Figure 4. CPTEC 500 mbar analysis of horizontal wind vectors at 0600, 1200, 1800, and 2400 UT on 3 August 2001 show persistent vigorous easterly flows of upper level wind fields. Little or no precipitation fell over most of the domain during this simulation period (Figure 5). On 4–6 August, persistent southeasterly trade winds advected dry air from northeastern Brazil into the Amazon Basin. Subsidence was present during this period, preventing measurable precipitation. During 10 to 12 August, weak squall lines developed when winds turned east-northeast, which favored convective activity [*Longo*, 2003].

4. Results

4.1. Model Evaluation: Near-Surface Meteorology and CO_2

[20] A comparison of near-surface meteorological fields and CO_2 concentration was carried out between the observations and the CO_2RAMS simulations for the period 1 August through 15 August 2001. The first available vertical level from the model is at 57 m. Available temperature observations for this period are from the Belterra meteorology tower at 2-m screen height, and the observed wind speed and direction are at 10 m. The modeled screen height temperature and 10-m wind speed are computed by the RAMS postprocessing routines based on *Louis* [1979] and *Louis et al.* [1982] similarity theory formulation over bare soil and vegetated surfaces. This scheme approximates the profile functions of *Businger et al.* [1971]; the parameterization of the horizontal and vertical diffusion coefficients is done using K-theory based on *Smagorinsky* [1963], where the mixing coefficients are related to the fluid deformation rate, and corrections are made to account for the influence of Brunt-Vaisala frequency [*Hill*, 1974] and Richardson number [*Lilly*, 1962].

[21] Figure 6 shows the comparison of 2-m screen height air temperature between the model and observations. The model agrees reasonably well with the observations, but with some cold biases, especially at midday. Over the entire

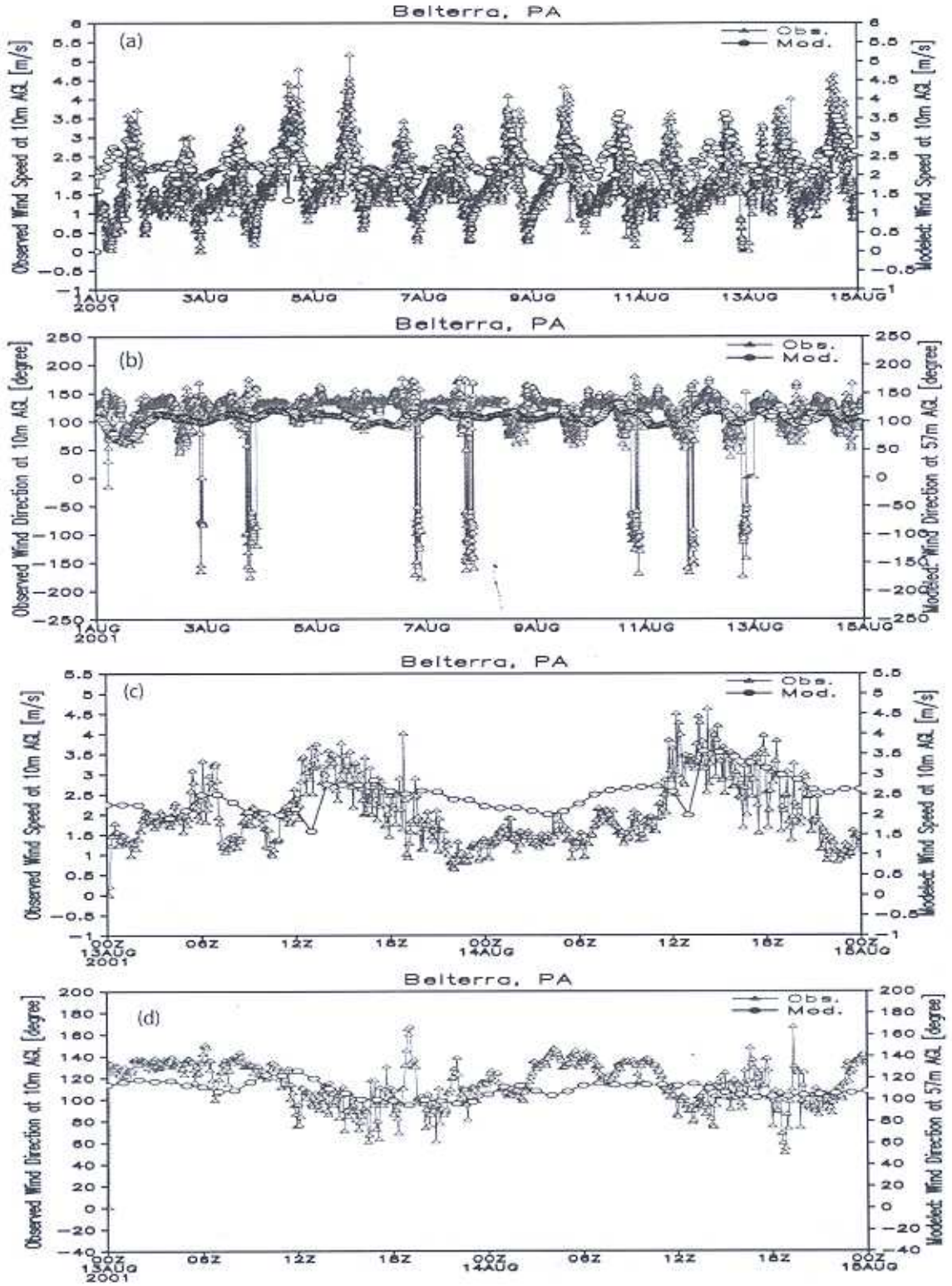

Figure 7. For the entire simulation time period from 0000 UT 1 August through 15 August 2001, (a) modeled versus observed wind speed at 10 m and (b) modeled (at 57 m) versus observed (at 10 m) wind direction. For the details from 0000 UT 13 August through 15 August 2001, (c) modeled versus observed wind speed at 10 m and (d) modeled (at 57 m) versus observed (at 10 m) wind direction. The times in the figure are in UT. The modeled output is at an hourly interval, while the observations are at a 5-min interval.

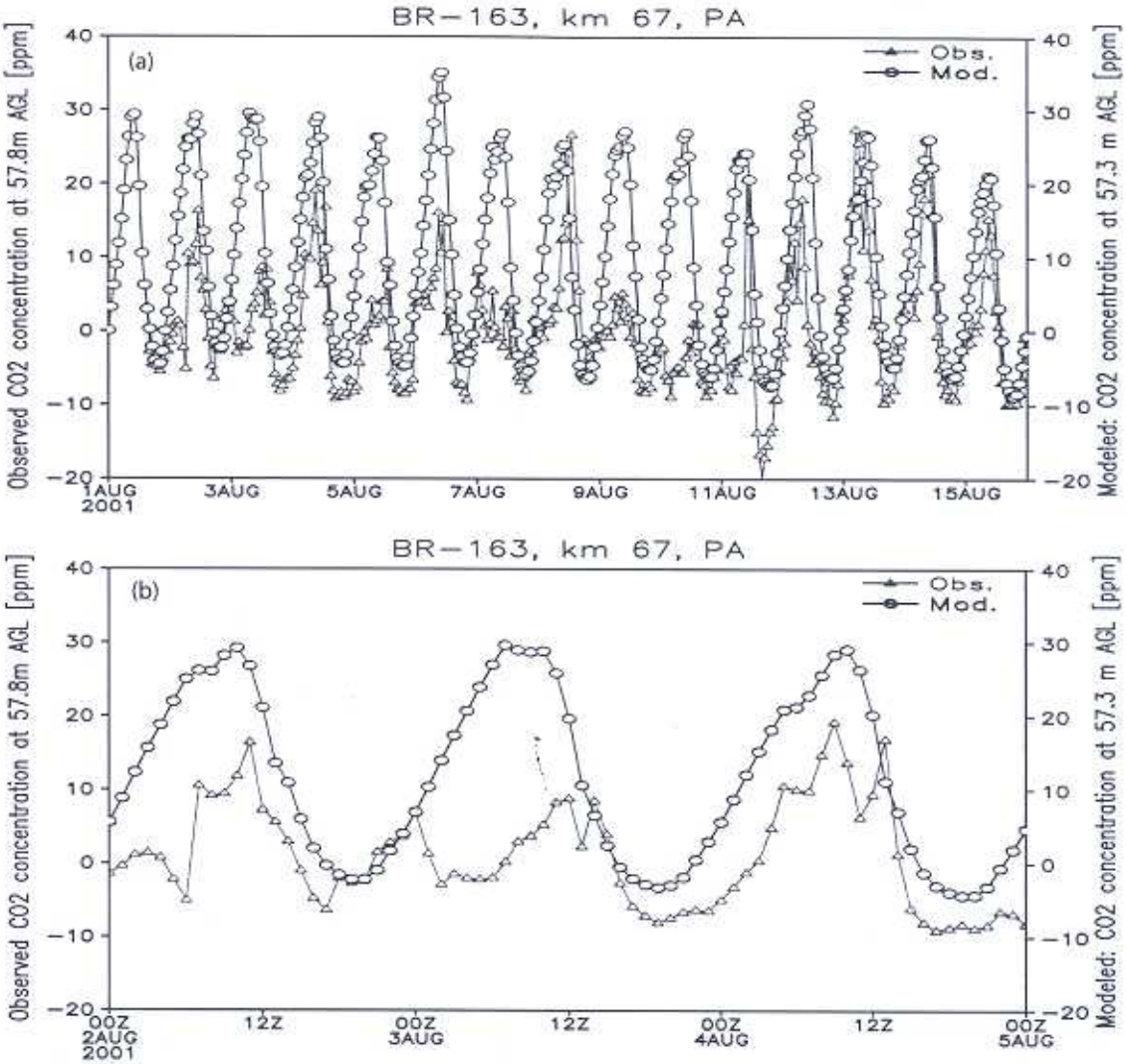

Figure 8. (a) Modeled versus observed CO_2 concentration anomaly at 57 m for the entire simulation time period from 0000 UT 1 August through 15 August 2001; (b) details of the same comparison as Figure 8a, but for 0000 UT 2 August through 5 August 2001. The times in the figure are in UT. The modeled output is at an hourly interval, while the observations are at a 30-min interval.

simulation time period, model-simulated T_{max} and T_{min} are, on average, 1.42°C and 0.25°C lower than observations, respectively, while the daily mean screen height air temperature is 0.61°C too low. The modeled temperature diurnal cycle is perfectly in phase with observations. The model tends to underestimate the screen height air temperature maxima but does a better job predicting minimum temperatures.

[22] The observed wind speed and direction comparisons are more divergent than that demonstrated with temperature. Figures 7a and 7b plot observed versus modeled values for the entire simulation period, while Figures 7c and 7d show the same comparison, but only for 13 and 14 August. The wind speed comparison is at 10 m, for both observation and model; while the wind direction comparison is at different levels: the observation is at 10-m level, and the model is at 57 m. The observed and modeled wind speeds average 1.78 m/s and 2.28 m/s, and the observed and modeled wind directions average 106.4° and 109.8°, respectively, for the entire simulation time period. Both observed and modeled winds demonstrate diurnal cycles. As expected, the nights are calm with more sporadic changes in wind directions; during the day, a strong southeasterly wind persists. The repeated slowdown of winds at 1300 UT (1000 local time (LT)) were simulated, and sometimes observed, as a result of the thermally driven land-river contrast. During that hour, the observed wind speed decreases are smaller than the modeled values, which indicates the model overestimated the differential heating. Both modeled and observed wind directions stay largely unchanged, i.e., there is no river-breeze-induced westerly flow. Overall, the general trends in observed wind speeds and directions are captured in the simulation, but the model overestimates the wind speeds, and has less southerly components compared to observations.

[23] Figure 8a displays the comparison of CO_2 concentration anomaly between model and Km 67 eddy flux tower, both at 57 m, which is above the top of the canopy. The observed CO_2 concentration anomalies are computed by subtracting the mean $[CO_2]$ from the time series. The

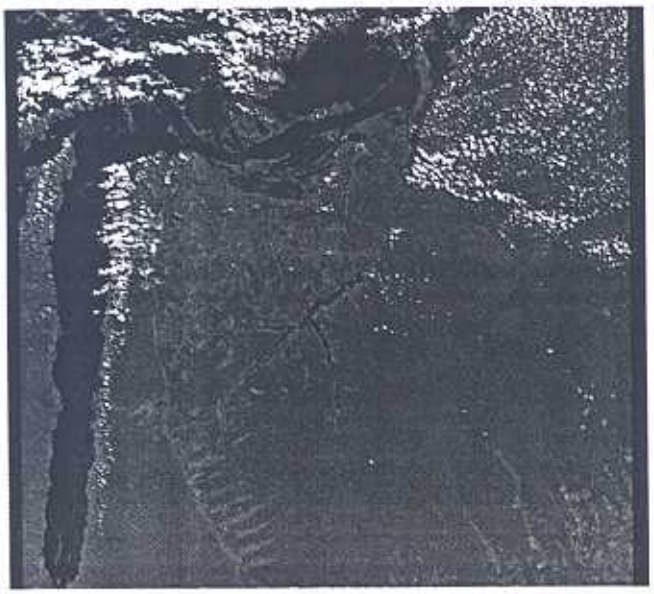

Figure 9. Satellite image obtained from LandSat 7 ETM+ scene for path 227 and row 62, on 31 July 2001. It shows that during a clear day, the low-level cumulus clouds favor the east bank of Tapajós River. The image is located at the Web site of Tropical Rain Forest Information Center (TRFIC), which is jointly hosted by LBA-ECO and Michigan State University.

observed [CO_2] is suppressed at night because of a stable nocturnal surface layer and a dense canopy structure. At night, CO_2 produced by soil respiration is trapped and accumulated below the canopy without reaching the instruments. Then early in the morning, solar heating breaks down the stable boundary layer and the initially shallow unstable surface layer starts to grow rapidly, supported by strong vertical mixing [*Stull*, 1988]. Within hours, the stored CO_2 under dense canopy is released in a "burst" and reaches the instrument, resulting in the observed early morning [CO_2] peaks, as shown in Figure 8b daily at 1200 to 1300 UT (0900 to 1000 LT). Because the model's first vertical level is at 57 m, which is above the canopy, the model cannot simulate these detailed intracanopy processes [*Denning et al.*, 2003]. Daytime [CO_2] agrees better with observations, but daily minima are slightly underestimated. The better agreement of [CO_2] maxima during the nights of 11 August through 15 August can be explained by the synoptic disturbance that happened on the night of 11 August, during which a weak squall line developed when large-scale background winds turned from southeast to northeast. Several met stations registered intermittent rainfall during those several days (as shown in Figure 5). The stronger than usual turbulent mixing during those nights may have allowed the canopy-trapped CO_2 to reach the instrument, resulting in better agreement between observations and model.

[24] In general, CO_2RAMS captures the diurnal variations relatively well, and is able to reproduce many aspects of the observed meteorology and CO_2 distributions. However, because of the model's coarse vertical resolution, and the difficulties of simulating intracanopy processes and stable nocturnal boundary conditions, the model misses some important details of observed features, such as early morning CO_2 flushing. The disparity in temperatures and winds between observed and modeled values likely involves scaling methodology applied. The model misses some synoptic signals, in part, because of inadequate representations of these features in the large-scale analysis product.

4.2. Low-Level Convergence Line Near the East Bank of Tapajós River

4.2.1. Satellite-Observed Cloud Band

[25] Shown in Figure 9 is a satellite image obtained from Landsat 7 ETM+ scene during the dry season. Low-level

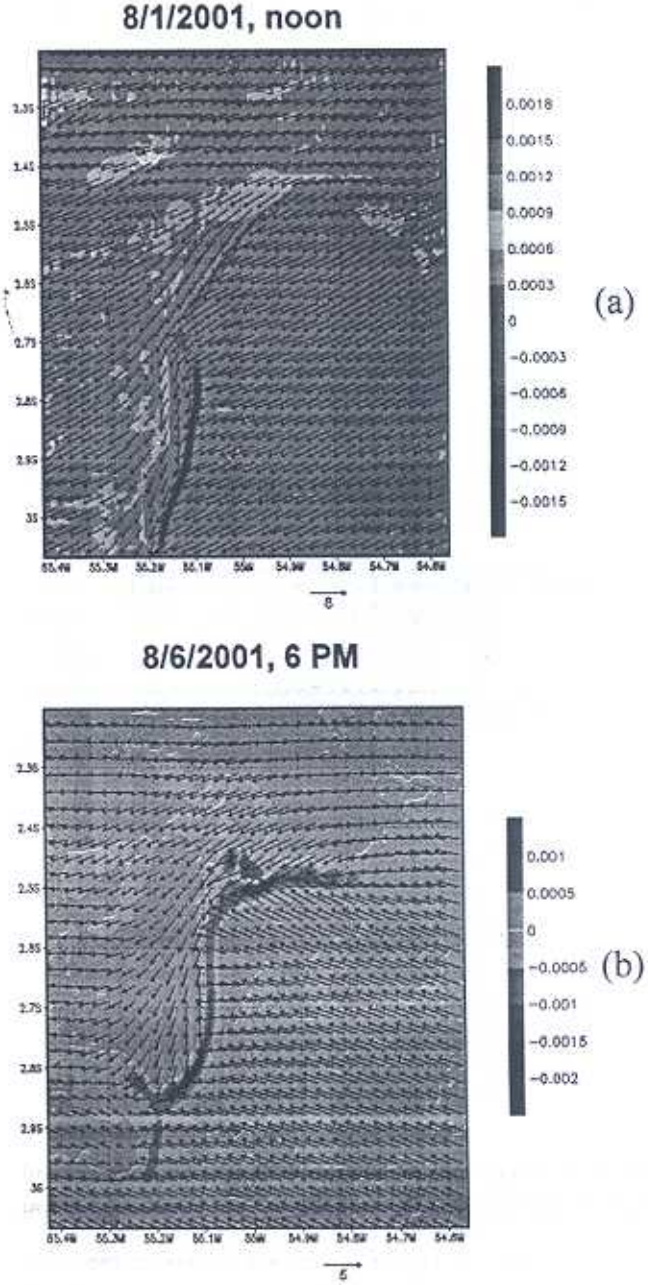

Figure 10. (a and b) Modeled horizontal wind vectors and surface divergences at 57 m (the model's first vertical level), at indicated times and days (local time).

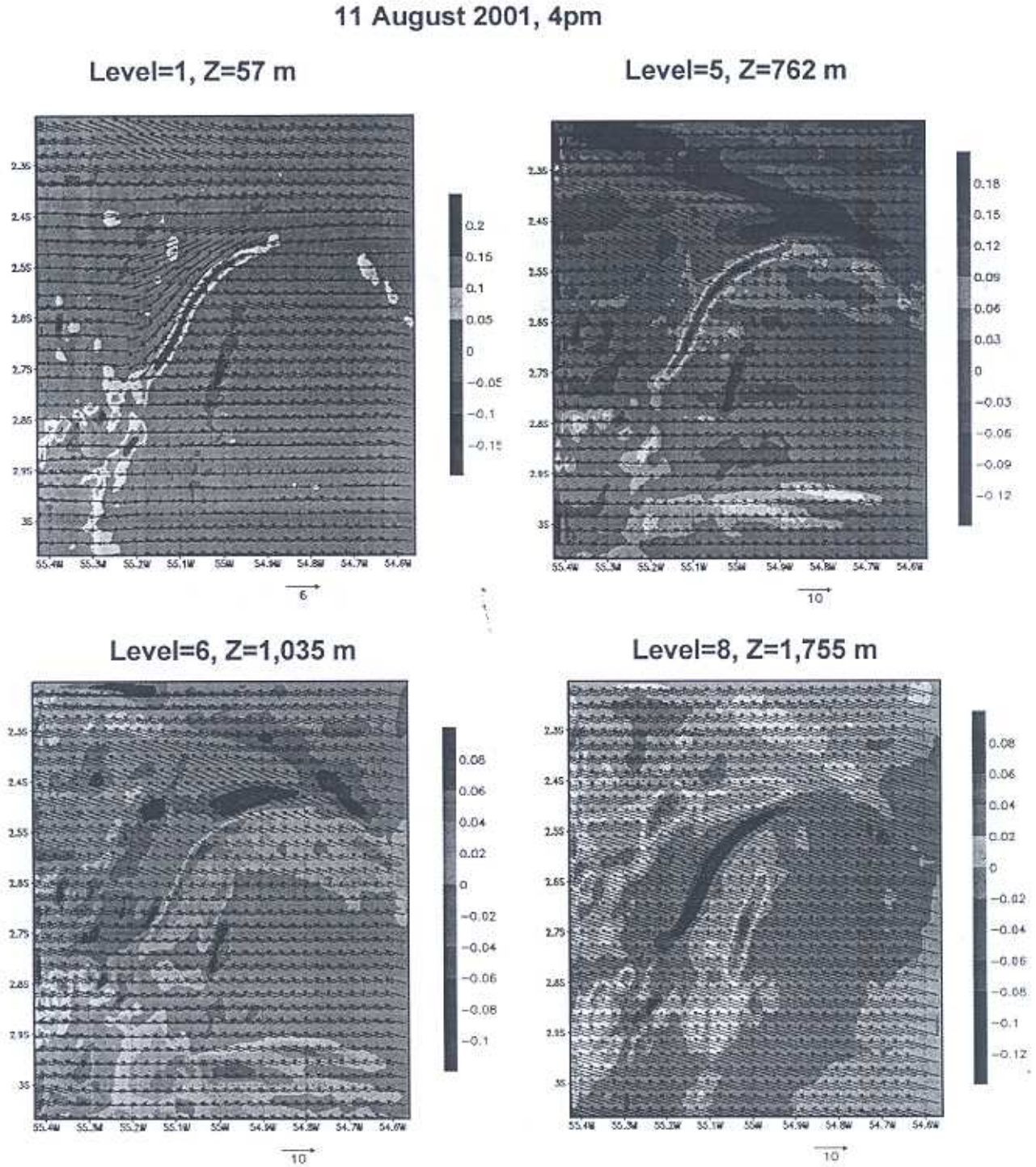

Figure 11. Modeled horizontal wind vectors and vertical velocities (color shades) at different model vertical levels, as indicated in the figure, on 11 August 2001, at 2000 UT (1600 LT).

cumulus clouds appear persistently in the study area, and seem to favor the east bank of the Tapajós River. This cloud band is frequently observed both by local people and in satellite imagery. The GOES satellite images of the same time period confirm similar patterns (figures not shown). Previous research has stressed the role of the thermally driven "river breeze" effect [*Oliveira and Fitzjarrald*, 1993, 1994; *Silva Dias et al.*, 2004]. This theory favors light wind conditions that prevail during trade wind breaks ("friagens"). However, the asymmetry and persistence of low-level cumulus clouds under strong trade wind conditions suggest that other mechanisms may be involved.

4.2.2. Simulated Low-Level Convergence Line

[26] Figures 10a and 10b show the modeled horizontal wind vectors and the surface divergence at 57 m (the first

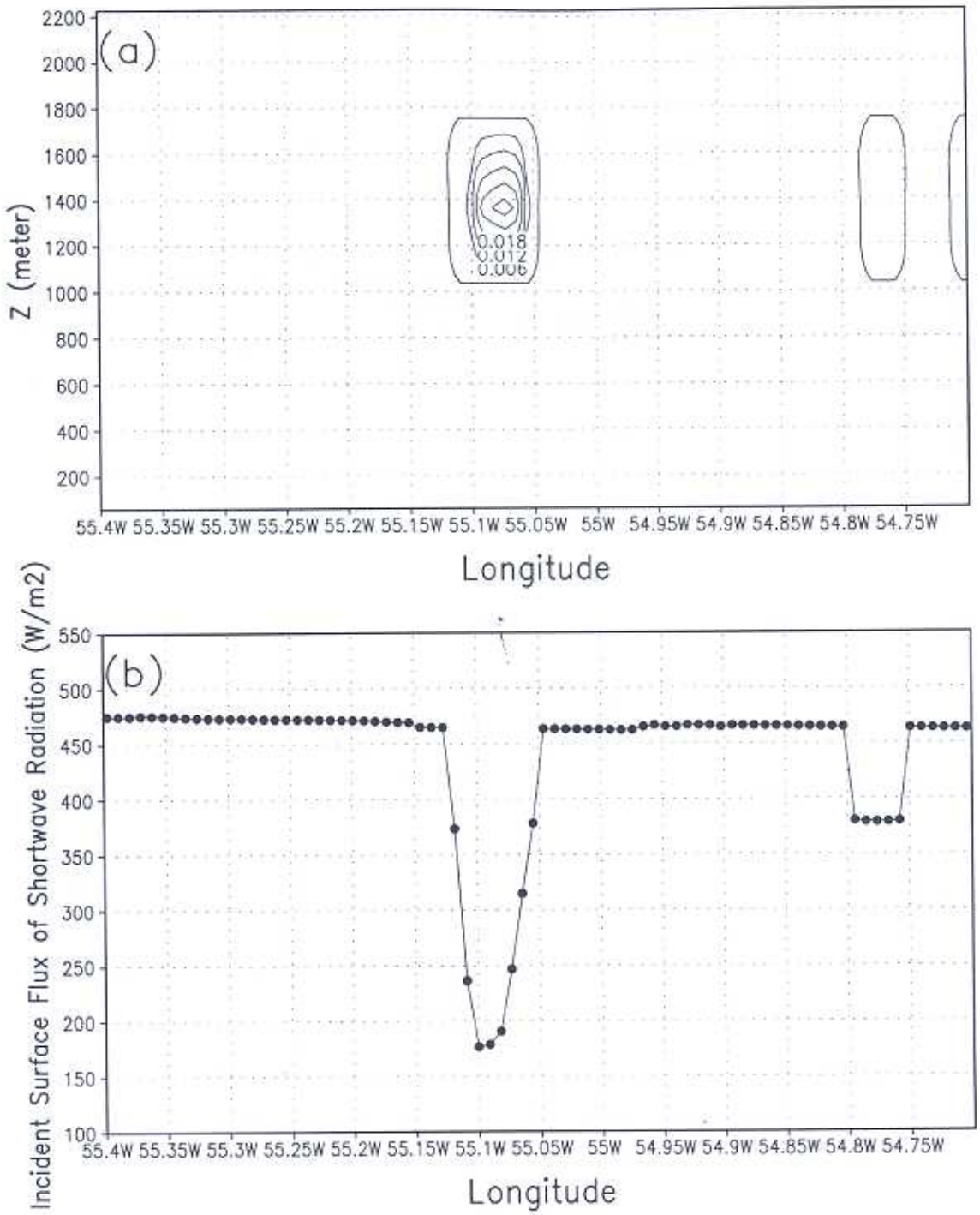

Figure 12. (a) Model-simulated cloud water mixing ratio (g/kg) at 1600 LT on 2 August 2001. The vertical cross section is taken at −2.8° latitude. (b) Model-simulated surface incoming shortwave radiation (W/m^2) at 1600 LT on 2 August 2001. The cross section is taken at −2.8° latitude. The Tapajós River is between −55.2° and −55.1° longitude.

model vertical level), on 1 August and 6 August 2001, at 1200 and 1800 LT, respectively. Although subsidence is present over nearly the entire domain, a narrow convergence line is formed along the east bank of the Tapajós River on each occasion at a slightly different location and time. This convergence line occurs twelve out of fifteen days during the simulation time period. The orientation of the convergence line steers perpendicularly against the background trade winds. The east bank of the Tapajós River is, indeed, a favorable place for each occurrence.

[27] Displayed in Figure 11 are the simulated horizontal wind vectors and vertical velocities, at 57 m, 762 m, 1035 m, and 1772 m heights, on 11 August 2001 at 1600 LT, showing the vertical structure of the convergence zone. At the first

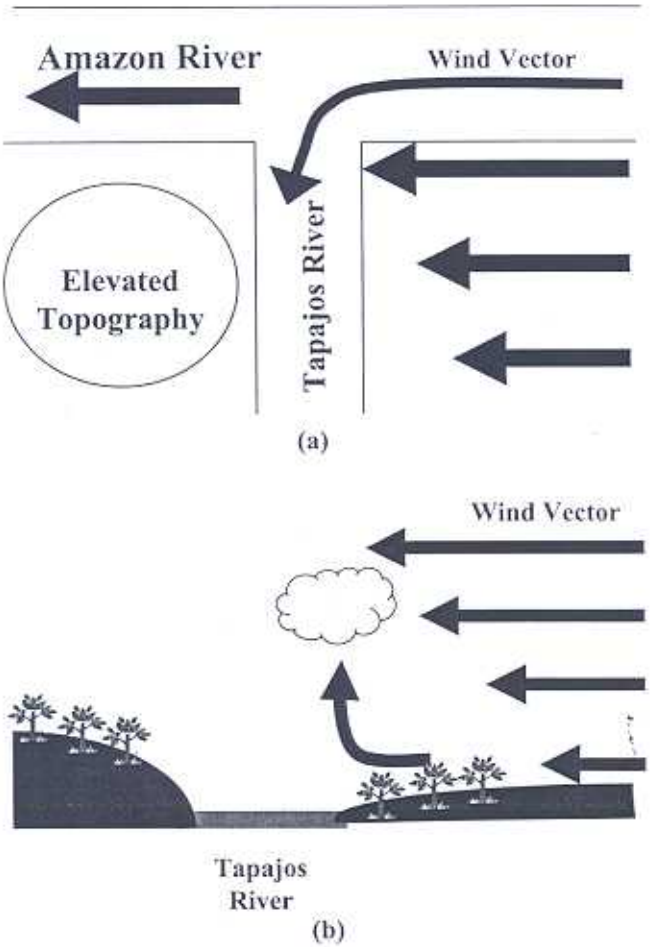

Figure 13. Conceptual diagram showing the mechanisms that lead to the low-level convergence line on the east bank of Tapajós River: (a) horizontal distribution and (b) vertical cross section.

model level, the near-surface convergence creates upward air motion. The rising air reaches the top of the boundary layer at around 1.7 km, leading to an upper level divergence, and this in turn, generates downward motion at that level.

[28] Shown in Figures 12a and 12b are model-simulated cloud water mixing ratio and surface incoming shortwave radiation at 1600 LT on 2 August 2001. Corresponding to the cloud formation, the model-simulated reduced incoming shortwave radiation, where the convergence zone forms; the model is able to capture the radiative effect of the convective cloud through the microphysics parameterization in the finest grid (grid 4, at 1-km grid spacing).

4.2.3. Possible Mechanisms for LLC

[29] These results prompt the question, "why are low-level cumulus clouds often better organized on the east bank of the Tapajós River?" We abstract the landscape features of our study area into two schematic diagrams illustrating this system's horizontal and vertical cross sections, as shown in Figures 13a and 13b. The elevated topography (~200 m) on the west bank of Tapajós River acts as a physical block to the surface winds, resulting in a north-south horizontal wind shear. The "T" shape juxtaposition of the Amazon and Tapajós Rivers, and the contrast in surface roughness length between the forest and the large rivers, tend to facilitate the turning of the lower-level winds from the Amazon to the Tapajós River. The channelized northerly flow along the Tapajós River produce directional convergence with the easterly trades as they reach the east bank, as evidenced in Figures 10a and 10b. The resulting convergence line produces upward motion reaching to between 1.5 to 2 km elevations, as shown in Figures 11 and 12a. These mechanically forced updrafts lead to increased cumulus clouds and sometimes precipitation.

4.2.4. Influence of LLC on Flux Tower NEE Observation

[30] Since three eddy covariance flux towers were built along the east bank of Tapajós River and Brazil Highway BR 163, an important question is: "Are the towers affected by the low-level convergence (LLC)?" And "if so, how does the LLC affect the CO_2 flux observations?" Displayed in Figure 14 are observed net ecosystem exchange (NEE) and Bowen ratio at flux tower Km 67 compared with simulated surface divergence at the same location from 3 August through 8 August 2001. Also shown is the observed net radiation from Belterra meteorological tower for the same time period. During the day, a midday NEE depression is frequently observed. However, plant vapor pressure deficit (VPD) can also lead to the increases in NEE because of reduced photosynthetic uptake [*Ghosh Hajra and Kumar*, 2002; *Gucci et al.*, 1996; *Cohen et al.*, 2000]. The Bowen ratio is defined as the sensible heat flux to the latent heat flux. If the plants were under VPD stress, increased sensible heat flux and decreased latent heat flux would result in a spike in observed Bowen ratio. On the other hand, the cloud-shading effect would reduce net radiation, in which would decrease both sensible and latent heat fluxes, leading to a relatively constant Bowen ratio. Figure 14 shows nearly constant Bowen ratios at midday. This suggests that water stress is not the cause of the midday NEE depression. The timing of the simulated midday cloudiness in the model is related to the maximum surface convergence. The observed net radiation from nearby Belterra meteorological tower confirms the existence of frequent midday cloudiness (Figure 14). To further examine how the LLC-induced cloudiness influences the observed CO_2 fluxes, photosynthetic active radiation (PAR) is plotted against NEE for the Km 67 flux tower, for a time period when both PAR and NEE are available. As shown in Figure 15, daytime cloudiness often leads to dips in PAR. Most of the time, when observed PAR decreases, NEE increases because of reduced photosynthetic uptake, as indicated by the vertical lines in the figure. If the flux towers are located at where the LLC occurs, the observed NEE can be frequently affected by the midday cloudiness, and therefore underestimate the carbon uptake when used to upscale to a larger region.

5. Summary and Discussion

[31] Mesoscale circulations and atmospheric CO_2 variations of Santarém area in Pará, Brazil, during the dry season 2001, were numerically investigated using CO_2RAMS with prescribed surface CO_2 fluxes according to land cover type. Model evaluation against flux tower observations and the SMC field measurements showed that, in many respects, the

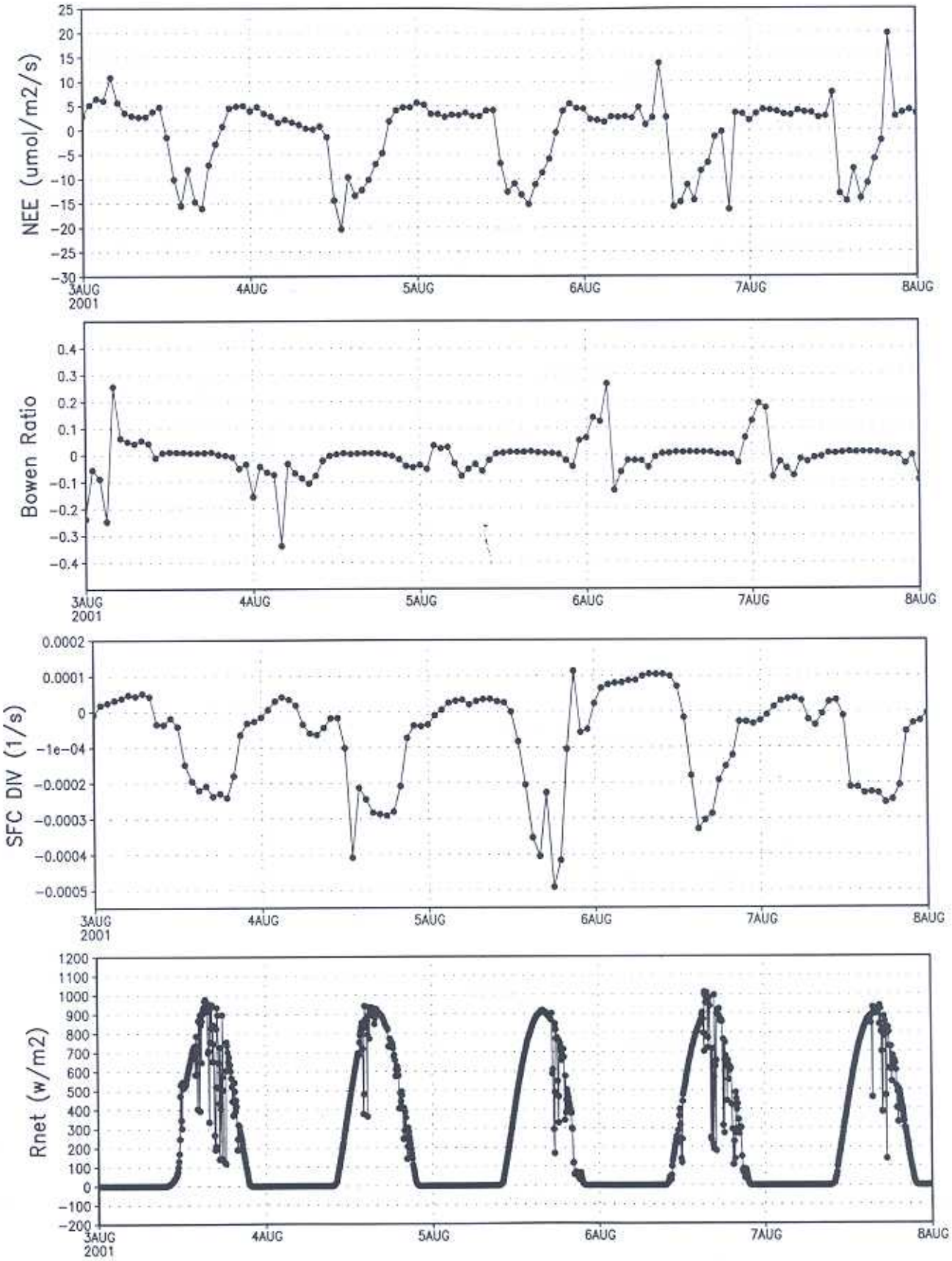

Figure 14. Observed net ecosystem exchange (NEE) and Bowen ratio at flux tower Km 67 compared with simulated surface divergence at the same location. Also shown is the observed net radiation at Belterra meteorological tower for the same time period.

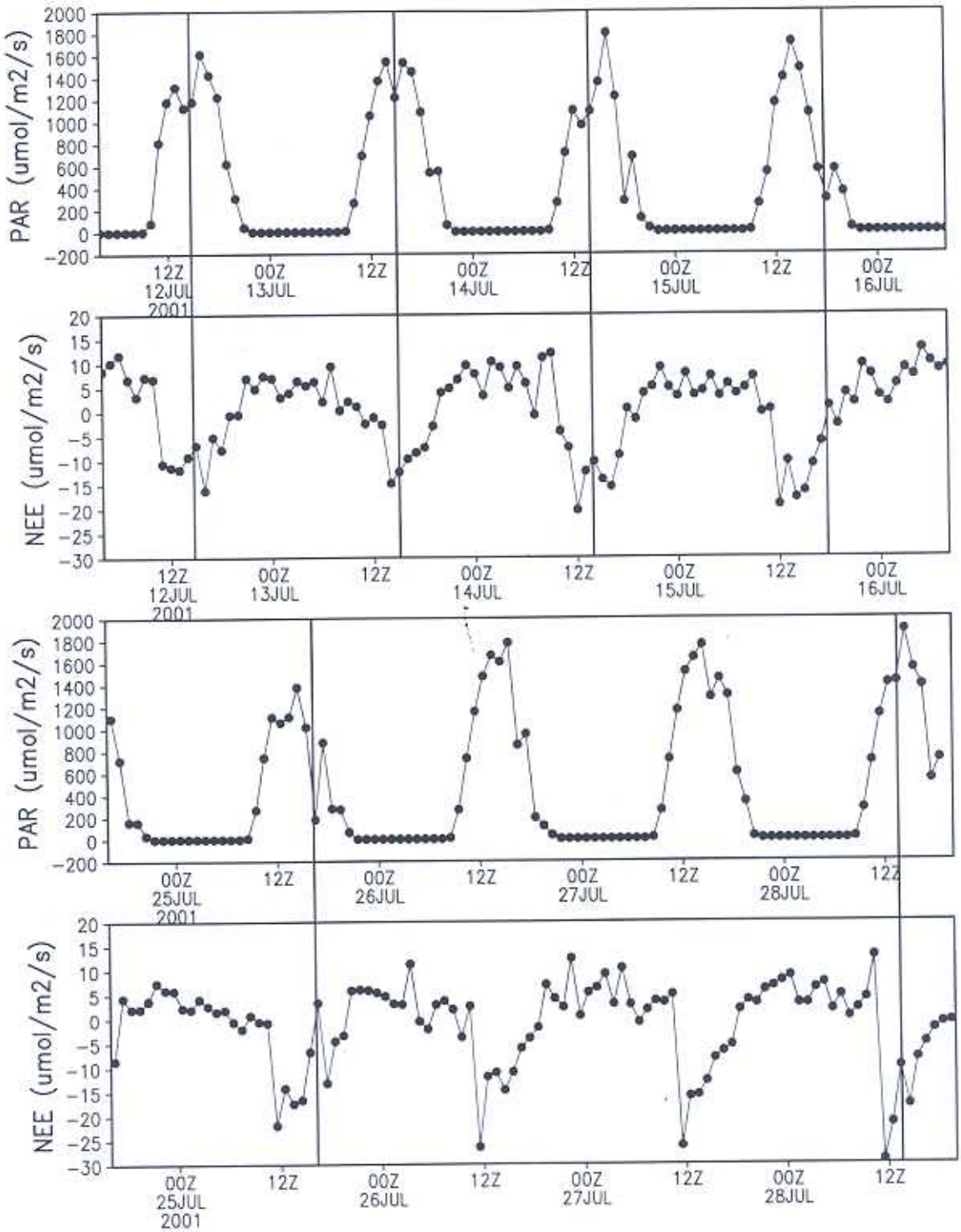

Figure 15. Observed photosynthetic active radiation (PAR) and net ecosystem exchange (NEE) at flux tower Km 67 during a time period when data are available.

model is doing a reasonable job simulating the observed meteorological variables and CO_2 concentrations. The model-observation discrepancies can largely be accounted for by the fact that the model simulates conditions above the canopy whereas the observations were taken near the surface.

[32] The mechanisms that lead to better organized low-level cumulus clouds on the east side of the Tapajós River were explored. The most significant finding is that low-level convergence zones occur not only during weak trade wind conditions, when thermally forced river breezes form, but are also evident on strong trade wind days. The numerical simulations illustrate that local topographic and landscape features, along with differences in roughness lengths between land and water, create a channeling effect that mechanically forces the surface winds to turn from the

Amazon to the Tapajós River. This subsequently leads to lower atmospheric wind to converge near the east side of Tapajós River. Differential heating between the land and water exists and has a strong diurnal cycle. However, the resulting river breezes are not strong enough to reverse the easterlies at the surface during the dry season strong-trade episode; it can only slow down the surface wind, and allow more upward transport of moisture from river to the cumulus clouds. The observed and simulated timings of LLC formation seem rather random. The lack of a predetermined diurnal cycle itself suggests the lesser importance of thermal forcing mechanism. The role of mechanical forcing versus thermal forcing in the formation of LLC deserves a detailed investigation in itself [*Lu et al.*, 2004]. We also performed a vorticity budget analysis, and found that solenoidal forcing associated with differential heating was not significant (figures not shown).

[33] The unique physical setting of the Tapajós National Forest with respect to both the juxtaposition of the large Amazon and Tapajós Rivers may produce a unique mesoscale and micrometeorological environment. The diurnal cycle of mean vertical motion, radiation, and precipitation during the dry season along the east bank of the Tapajós River is substantially influenced by the unique geographic setting through a mechanically forced low-level convergence zone. Systematic diurnal variations in mean vertical velocity may have implications for the calculation of turbulent fluxes of heat, momentum, water, and carbon [*Baldocchi*, 2003]. The simultaneous enhancement of diffuse light, humidity, and vertical motion at midday probably also influences the vertical distribution of atmospheric CO_2, and must be treated correctly in regional inverse modeling efforts. It is also possible that the evolution of the forest ecosystem in the region reflects adaptation to enhanced midday cloudiness and/or precipitation relative to similar forests nearby. If so, the effects of mesoscale circulations and associated patterns of radiation, humidity, and precipitation should be accounted for when generalizing from flux tower data or upscaling to a larger region.

[34] A better understanding of mesoscale circulations, advection, storage and drainage processes are important in the interpretation of eddy flux measurements. To quantify how CO_2 fluxes, the underlying vegetation, and the flux footprint vary with meteorological conditions, plant physiological and biogeochemical processes need to be included. As a next step in this research, a coupled SiB2-RAMS model, which can dynamically simulate the vegetation CO_2 flux responses to meteorological variations, such as cloudiness, and wind directions, will be employed, to show how both biological controls and meteorological factors influence regional-scale CO_2 prediction.

[35] Finally, our numerical study suggests that detailed, high-resolution, mesoscale studies need to be undertaken for other long-term monitoring sites as well. Coarser resolution simulations will likely misinterpret various signals in CO_2 fluxes and concentrations at Santarem. Mesoscale numerical experiments can be a powerful tool to help determine the unique meteorological conditions associated with each tower, and to evaluate and identify the possible sources of systematic bias of tower measurements.

[36] **Acknowledgments.** This research was sponsored by NASA LBA-Ecology, grant NCC5-284, entitled "Spatial Integration of Regional Carbon Balance in Amazonia." We thank Steven Wofsy for his support in providing Km 67 tower data for our analysis and Ricardo Sakai and David Fitzjarrald for providing Km 77 tower data. We obtained Km 83 tower data from the Ameriflux Web site. Special thanks go to Yiqi Luo for his insightful discussion, J. C. Lin for his constructive comments and G. E. Liston for his thorough edits, which, as a result, greatly improved our manuscript. Part of this work was also funded by FAPESP and the Ministry of Science and Technology in Brazil through the Millennium Institute program.

References

Arakawa, A., and R. V. Lamb (1977), Computational design of the basic dynamical processes of the UCLA general circulation model, *Methods Comput. Phys.*, *17*, 174–265.

Avissar, R., and R. A. Pielke (1989), A parameterization of heterogeneous land surfaces for atmospheric numerical models and its impact on regional meteorology, *Mon. Weather Rev.*, *117*(10), 2113–2136.

Baldocchi, D. D. (2003), Assessing the eddy covariance technique for evaluating carbon dioxide exchange rates of ecosystems: Past, present and future, *Global Change Biol.*, *9*, 479–492.

Baldocchi, D. D., et al. (2001), FLUXNET: A new tool to study the temporal and spatial variability of ecosystem-scale carbon dioxide, water vapor and energy flux densities, *Bull. Am. Meteorol. Soc.*, *82*, 2415–2434.

Band, L. E. (1993), Effect of land surface representation on forest water and carbon budgets, *J. Hydrol.*, *150*, 749–772.

Businger, J. A., J. C. Wyngaard, Y. Izumi, and E. F. Bradley (1971), Flux-profile relationship in the atmosphere surface layer, *J. Atmos. Sci.*, *28*, 181–189.

Chen, F., R. A. Pielke Sr., and K. Mitchell (2001), Development and application of land-surface models for mesoscale atmospheric models: Problems and promises, in *Observation and Modeling of the Land Surface Hydrological Processes, Water Sci. Appl.*, vol. 3, edited by V. Lakshmi, J. Alberston, and J. Schaake, pp. 107–135, AGU, Washington, D. C.

Clark, T. L. (1977), A small-scale dynamic model using a terrain-following coordinate transformation, *J. Comput. Phys.*, *24*, 186–215.

Cohen, S., A. Grava, and E. E. Goldschmidt (2000), Citrus response to radiation load reduction: Water use, photosynthesis, and productivity, paper presented at 9th International Citrus Congress, Univ. of Fla. Inst. of Food and Agric. Sci. Citrus Res. and Educ. Cent., Orlando, Fla.

Cotton, W. R., et al. (2003), RAMS 2001: Current status and future directions, *Meteorol. Atmos. Phys.*, *82*, 5–29.

Denning, S. A., M. Nicholls, L. Prihodko, I. Baker, P. L. Vidale, K. Davis, and P. Bakwin (2003), Simulated variations in atmospheric CO_2 over a Wisconsin forest using a coupled ecosystem-atmosphere model, *Global Change Biol.*, *9*, 1241–1250.

Dickinson, R. E. (1987), *The Geophysiology of Amazonia: Vegetation and Climate Interactions*, 1st ed., 526 pp., John Wiley, Hoboken, N. J.

Freitas, S. R., M. A. F. Silva Dias, P. L. Siva Dias, K. M. Longo, P. Artaxo, M. O. Andreae, and H. Fischer (2000), A convective kinematic trajectory technique for low-resolution atmospheric models, *J. Geophys. Res.*, *105*(D19), 24,375–24,386.

Freitas, S. R., K. M. Longo, M. A. F. Silva Dias, P. L. Silva Dias, R. Chatfield, E. Prins, P. Artaxo, G. Grell, and F. S. Recuero (2005), Monitoring the transport of biomass burning emissions in South America, *Environ. Fluid Mech.*, *5*(1–2), doi:10.1007/s10652-005-0243-7.

Ghosh Hajra, H., and R. Kumar (2002), Diurnal and seasonal variations in gas exchange property of tea leaves, *J. Plant Biol.*, *29*(2), 160–173.

Gucci, R., R. Massai, C. Xiloyannis, and J. A. Flore (1996), The effect of drought and vapour deficit on gas exchange of young kiwifruit (*Actinidia deliciosa* var. deliciosa) vines, *Ann. Bot.*, *77*, 605–613.

Hahmann, A. N., and R. E. Dickinson (2001), A fine-mesh land approach for general circulation models and its impact on regional climate, *J. Clim.*, *14*(7), 1634–1646.

Hamilton, M. G., and J. R. Tarifa (1978), Synoptic aspects of a polar outbreak leading to frost in tropical Brazil, July, 1972, *Mon. Weather Rev.*, *106*, 1545–1556.

Harrington, J. Y., T. Reisin, W. R. Cotton, and S. M. Kreidenweis (1999), Cloud resolving simulations of Arctic stratus. Part II: Transition-season clouds, *Atmos. Res.*, *51*, 45–75.

Harrington, J. Y., G. Feingold, and W. R. Cotton (2000), Radiative impacts on the growth of a population of drops within simulated summertime arctic stratus, *J. Atmos. Sci.*, *57*, 766–785.

Hill, G. E. (1974), Factors controlling the size and spacing of cumulus clouds as revealed by numerical experiments, *J. Atmos. Sci.*, *31*, 646–673.

Lilly, D. K. (1962), On the numerical simulation of buoyant convection, *Tellus*, *14*(2), 148–172.

Liu, Y., C. Weaver, and R. Avissar (1999), Toward a parameterization of mesoscale fluxes and moist convection induced by landscape heterogeneity, *J. Geophys. Res.*, *104*(D16), 19,515–19,534.

Longo, M. (2003), Horizontal vorticity budget associated with a mesoscale convective system in Amazon Basin (in Portuguese), M.S. dissertation, 133 pp., Univ. de São Paulo, Brazil.

Louis, J. F. (1979), A parametric model of vertical eddy fluxes in the atmosphere, *Boundary Layer Meteorol.*, *17*, 187–202.

Louis, J. F., M. Tiedtke, and J. F. Geleyn (1982), A short history of the PBL parameterization at ECMWF, in *Proceedings of the 1981 Workshop on PBL Parameterization*, pp. 59–71, Eur. Cent. for Medium-Range Weather Forecasts, Reading, UK.

Loveland, T. R., B. C. Reed, J. F. Brown, D. O. Ohlen, J. Zhu, L. Yang, and J. Merchant (2000), Development of a Global Land Cover Characteristics Database and IGBP DISCover from 1-km AVHRR data, *Int. J. Remote Sens.*, *21*(6/7), 1303–1330.

Lu, L., and W. J. Shuttleworth (2002), Incorporating NDVI-derived LAI into the climate version of RAMS and its impact on regional climate, *J. Hydrometeorol.*, *3*, 347–362.

Lu, L., R. A. Pielke, G. E. Liston, W. J. Parton, D. Ojima, and M. Hartman (2001), Implementation of a two-way interactive atmospheric and ecological model and its application to the central United States, *J. Clim.*, *14*, 900–919.

Lu, L., A. S. Denning, M. A. Silva Dias, P. Silva Dias, and M. Longo (2004), Why the lower level cumulus clouds are often better organized on the east bank of Tapajós River?: A mechanistic study, paper presented at AMS Annual Meeting, Am. Meteorol. Soc., Seattle, Wash., Jan.

Ludwig, R., M. Probeck, and W. Mauser (2003), Mesoscale water balance modelling in the upper Danube watershed using sub-scale land cover information derived from NOAA-AVHRR imagery and GIS-techniques, *Phys. Chem. Earth*, *28*(33–36), 1351–1364.

Marengo, J. A., A. Cornejo, P. Satyamurty, C. Nobre, and W. Sea (1997), Cold surges in tropical and extratropical South America: The strong event in June 1994, *Mon. Weather Rev.*, *125*, 2759–2786.

Nicholls, M. E., A. S. Denning, L. Prihdodko, P. L. Vidale, I. Baker, K. Davis, and P. Bakwin (2004), A multiple-scale simulation of variations in atmospheric carbon dioxide using a coupled biosphere-atmospheric model, *J. Geophys. Res.*, *109*, D18117, doi:10.1029/2003JD004482.

Oliveira, A. P., and D. R. Fitzjarrald (1993), The Amazon River breeze and the local boundary-layer: 1. Observations, *Boundary Layer Meteorol.*, *63*(1–2), 141–162.

Oliveira, A. P., and D. R. Fitzjarrald (1994), The Amazon River breeze and the local boundary layer: 2. Linear-analysis and modeling, *Boundary Layer Meteorol.*, *67*(1–2), 75–96.

Pielke, R. A. (2001), Influence of the spatial distribution of vegetation and soils on the prediction of cumulus convective rainfall, *Rev. Geophys.*, *39*, 151–177.

Pielke, R. A., G. Dalu, J. S. Snook, T. J. Lee, and T. G. F. Kittel (1991), Nonlinear influence of mesoscale land use on weather and climate, *J. Clim.*, *4*, 1053–1069.

Pielke, R. A., et al. (1992), A comprehensive meteorological modeling system RAMS, *Meteorol. Atmos. Phys.*, *49*, 69–91.

Pielke, R. A., D. S. Schimel, T. J. Lee, T. G. F. Kittel, and X. Zeng (1993a), Atmosphere-terrestrial ecosystem interactions: Implications for coupled modeling, *Ecol. Modell.*, *67*, 5–18.

Pielke, R. A., J. H. Rodriguez, J. L. Eastman, R. L. Walko, and R. A. Stocker (1993b), Influence of albedo variability in complex terrain on mesoscale systems, *J. Clim.*, *6*, 1798–1806.

Pielke, R. A., R. Avissar, M. Raupach, H. Dolman, X. Zeng, and S. Denning (1998), Interactions between the atmosphere and terrestrial ecosystems: Influence on weather and climate, *Global Change Biol.*, *4*, 461–475.

Pielke, R. A., R. L. Walko, L. Steyaert, P. L. Vidale, G. E. Liston, and W. A. Lyons (1999a), The influence of anthropogenic landscape changes on weather in south Florida, *Mon. Weather Rev.*, *127*, 1663–1673.

Pielke, R. A., G. E. Liston, J. L. Eastman, L. Lu, and M. Coughenour (1999b), Seasonal weather prediction as an initial value problem, *J. Geophys. Res.*, *104*, 19,463–19,479.

Richey, J. E., J. I. Hedges, A. H. Devol, and P. D. Quay (1990), Biogeochemistry of carbon in the Amazon River, *Limnol. Oceanogr.*, *35*(2), 352–371.

Richey, J. E., J. M. Melack, A. K. Aufdenkampe, V. M. Ballester, and L. Hess (2002), From water to the atmosphere: Carbon dioxide evasion from the Amazon River system, *Nature*, *416*, 617–620.

Saatchi, S. S., B. Nelson, E. Podest, and J. Holt (2000), Mapping land cover types in the Amazon Basin using 1 km JERS-1 mosaic, *Int. J. Remote Sens.*, *21*(6–7), 1201–1234.

Saleska, S. R., et al. (2003), Carbon in Amazon forests: Unexpected seasonal fluxes and disturbance-induced losses, *Science*, *302*, 1554–1557.

Silva Dias, M. A. F., P. L. Silva Dias, M. Longo, D. R. Fitzjarrald, and A. S. Denning (2004), River breeze circulation in eastern Amazon: Observations and modeling results, *Theor. Appl. Climatol.*, *78*(1–3), 111–121.

Smagorinsky, J. (1963), General circulation experiments with the primitive equations: Part I. The basic experiment, *Mon. Weather Rev.*, *91*, 99–164.

Stohl, A., G. Wotawa, P. Seibert, and H. Kromp-Kolb (1995), Interpolation errors in wind fields as a function of spatial and temporal resolution and their impact on different types of kinematic trajectories, *J. Appl. Meteorol.*, *34*, 2149–2165.

Stohlgren, T. J., T. N. Chase, R. A. Pielke Sr., T. G. F. Kittel, and J. Baron (1998), Evidence that local land use practices influence regional climate, vegetation, and stream flow patterns in adjacent natural areas, *Global Change Biol.*, *4*, 495–504.

Stull, R. B. (1988), *An Introduction to Boundary Layer Meteorology*, Springer, New York.

Tremback, C. J. (1990), Numerical simulation of a mesoscale convective complex: Model development and numerical results, Ph.D. dissertation, 247 pp., Colo. State Univ., Fort Collins.

Tripoli, G. J., and W. R. Cotton (1980), A numerical investigation of several factors contributing to the observed variable intensity of deep convection over south Florida, *J. Appl. Meteorol.*, *19*, 1037–1063.

Tripoli, G. J., and W. R. Cotton (1982), The Colorado State University three-dimensional cloud/mesoscale model–1982, Part I: General theoretical framework and sensitivity experiments, *J. Rech. Atmos.*, *16*, 185–220.

Walko, R. L., W. R. Cotton, M. P. Meyers, and J. Y. Harrington (1995), New RAMS cloud microphysics parameterization, Part I: The single-moment scheme, *Atmos. Res.*, *38*, 29–62.

Walko, R. L., et al. (2000), Coupled atmosphere-biosphysics-hydrology model models for environmental modeling, *J. Appl. Meteorol.*, *39*, 931–944.

Xue, Y., F. J. Zeng, K. E. Mitchell, Z. Janjic, and E. Rogers (2001), The impact of land surface processes on simulations of the U.S. hydrological cycle: A case study of the 1993 flood using the SSiB land surface model in the NCEP Eta regional model, *Mon. Weather Rev.*, *129*(12), 2833–2860.

M. A. da Silva-Dias, P. da Silva-Dias, and M. Longo, Department of Atmospheric Sciences, University of São Paulo, São Paulo 05508-900, Brazil.

A. S. Denning and L. Lu, Department of Atmospheric Science, Colorado State University, Fort Collins, CO 80525, USA. (lixin@atmos.colostate.edu)

S. R. Freitas, Centre for Weather Forecasting and Climate Studies, National Institute for Space Research, CEP 12630-000, Cachoeira Paulista, Brazil.

S. Saatchi, NASA Jet Propulsion Laboratory, 4800 Oak Grove Drive, Pasadena, CA 91109, USA.